HHS Public Access

Author manuscript

Cancer Immunol Res. Author manuscript; available in PMC 2022 July 29.

Published in final edited form as:

Cancer Immunol Res. 2018 May ; 6(5): 566–577. doi:10.1158/2326-6066.CIR-17-0543.

Caspase-1 from Human Myeloid Derived Suppressor Cells Can Promote T cell–Independent Tumor Proliferation

Qi Zeng[1,#], **Juan Fu**[2,#], **Michael Korrer**[5], **Mikhail Gorbounov**[1], **Peter J. Murray**[4], **Drew Pardoll**[2], **David L. Masica**[3], **Young J. Kim**[5,6,*]

[1]Johns Hopkins School of Medicine, Johns Hopkins Hospital, Baltimore, MD

[2]Bloomberg-Kimmel Institute for Cancer Immunotherapy, Johns Hopkins Hospital, Baltimore, MD

[3]Department of Biomedical Engineering and Institute for Computational Medicine, Johns Hopkins Hospital, Baltimore, MD

[4]Max-Planck Institute of Biochemistry, Germany

[5]Department of Otolaryngology-Head & Neck Surgery, Vanderbilt University Medical Center, Nashville, TN.

[6]Vanderbilt-Ingram Cancer Center, Vanderbilt University Medical Center, Nashville, TN.

Abstract

Immunosuppressive myeloid-derived suppressive cells (MDSCs) are characterized by their phenotypic and functional heterogeneity. To better define their T cell–independent functions within the tumor, sorted monocytic $CD14^{+}CD11b^{+}HLA\text{-}DR^{low/-}$ MDSCs (mMDSCs) from squamous cell carcinoma patients showed upregulated caspase-1 activity, that was associated with increased IL1β and IL18 expression. *In vitro* studies demonstrated that mMDSCs promoted caspase-1–dependent proliferation of multiple squamous carcinoma cell lines in both human and murine systems. *In vivo*, growth rates of B16, MOC1, and Panc02 were significantly blunted in chimeric mice adoptively transferred with caspase-1 null bone marrow cells under T cell–depleted conditions. Adoptive transfer of wildtype $Gr\text{-}1^{+}CD11b^{+}$ MDSCs from tumor-bearing mice reversed this antitumor response, whereas caspase-1 inhibiting thalidomide-treated MDSCs phenocopied the antitumor response found in caspase-1 null mice. We further hypothesized that MDSC caspase-1 activity could promote tumor intrinsic MyD88-dependent carcinogenesis. In mice with wildtype caspase-1, MyD88-silenced tumors displayed reduced growth rate, but in chimeric mice with caspase-1 null bone marrow cells, MyD88-silenced tumors did not display differential tumor growth rate. When we queried the TCGA database, we found that caspase-1 expression is correlated with overall survival in squamous cell carcinoma patients. Taken together, our findings demonstrated that caspase-1 in MDSCs is a direct T cell–independent mediator of tumor proliferation.

[*]Corresponding Author: Young J. Kim, MD, PhD, FACS, Barry & Amy Baker Endowed Chair, Director, Head & Neck Oncologic Research, Co-Leader, Translational Research and Interventional Oncology, Vanderbilt-Ingram Cancer Center, Dept. Otolaryngology – Head & Neck Surgery, Vanderbilt University, School of Medicine, Nashville, TN, 37232, Phone: 615-343-8848, Fax: 615-343-9556, y2.kim@vanderbilt.edu.

[#]These authors contributed equally to the work

Conflict of Interest: none

Keywords

squamous cell carcinoma; MDSC; caspase-1; inflammasome complex; NF-kB

Introduction

Myeloid derived suppressor cells (MDSCs) are immature myeloid cells that have been functionally defined by their ability to suppress T cells in tumor-bearing mice, as well as cancer patients (1, 2). Depletion of L-arginine and cysteine, increased nitric oxide (NO), upregulation of reactive oxygen species (ROS), peroxynitrates, and multiple cytokines appear to mediate MDSCs' T cell–suppressive function (3–6). As a heterogeneous cell population, however, MDSCs' role as a key mediator of tumor progression has expanded (7–11). These lines of evidence have converged with others who have shown that abnormal myelopoiesis and recruitment of immature myeloid cells intended for inflamed tissue promote cancer cell proliferation by various mechanisms (12–14). We previously showed that STAT3 signaling in human MDSCs can regulate immunosuppressive function of MDSCs, and some of the downstream STAT3-dependent cytokines have been characterized as potentially mitogenic, particularly IL6 (15–17). Other myeloid-derived cytokines, such as IL1β and TGFβ, have been implicated in promoting carcinogenesis (8, 18–20), but these were noted to be primarily T cell–dependent processes. What has not been clear is MDSCs' non–T cell–dependent role in the human tumor microenvironment (TME). Tumors that are refractory to immune checkpoint inhibitors tend to be T-cell poor (21–23), so understanding MDCSs' T cell–independent, pro-carcinogenic mechanisms are important for the future development of combinatorial immuno-oncologic trials. Although clinical trials targeting MDSCs and tumor-associated macrophages (TAMs) are ongoing (24, 25), how these tumor-infiltrating myeloid cells shape the tumor in a T-cell poor TME may direct the next wave of combinatorial immunotherapies (26).

The crosstalk between cancer cells and myeloid cells in the context of inflammation-induced tumorigenesis demonstrated that inflammasomes and MyD88 play an important role in murine $Apc^{min/+}$ models (27). IL1β and IL18 have a protective role in MyD88-dependent neoplastic development in some of these murine models (28, 29). The NLRP3 inflammasome complex, in some colorectal carcinoma models, can confer an anti-carcinogenic effect (30–34). However, other murine models in gastric cancers, B16F10 melanoma, colitis-associated colon cancer, and T-ALL have variously shown opposing pro-tumorigenic activities of inflammasome cytokines (35, 36). Chemotherapy can further confound the picture to activate the NLRP3 inflammasome to promote tumor growth rate (37). In short, the literature points to context-dependent roles of inflammasomes in cancer biology. Many of these inflammation-associated tumorigenesis models have been focused on tumor intrinsic inflammasomes, and it is unclear how the tumor cell extrinsic inflammasome/capase-1 axis can regulate tumor cells directly.

To resolve some of this complexity, particularly as to how it relates to human cancer, we focused on the expression and function of caspase-1 in MDSCs from head & neck squamous cell carcinoma (HNSCC) patients. Using both human *in vitro* and murine *in*

vivo models, we found that caspase-1 from MDSCs can promote T cell–independent, pro-carcinogenic effects on cancer cells. This report underscores the role of tumor-infiltrating MDSCs as a key regulator of the TME, with both T cell–independent and T cell–dependent pro-carcinogenic effects, supporting clinical trials targeting caspase-1 and IL1β in solid tumors associated with MDSCs and adds to the body of evidence to potentially warrant changes in the nomenclature of MDSCs.

Materials and Methods

Study approval

Our study was performed in compliance with approved Johns Hopkins Hospital and Vanderbilt University Medical Center Institutional Review Board protocols in accordance with the Belmont Report. All subjects provided written informed consent prior to participation, and the specimens were de-identified prior to analysis. Included were HNSCC patients undergoing surgery for curative intent. Excluded were those with autoimmune diseases and chronic steroid use. Fresh tumor specimens (typically $1cm^3$) were harvested from non-margin areas and processed in PBS within 2 hours of resection.

Reagents and Cells

Cell Proliferation Dye eFluor 450 ™ (eBioscience) was used for cell proliferation assays, according to the manufacturer's protocol. Anti-human CD11b-PE (clone ICRF44), anti-human HLA-DR (clone, G46–6)-FITC, anti-human CD14–PerCP-Cy5.5 (clone, mφP9), anti-mouse Gr-1–Alexa Fluor 700 (Biolegend, clone: RB6–8cC5), anti-mouse CD11b–PE-Cy7(clone: M1/70) and Ly-6C-PE (clone AL-21) were obtained from BD Pharmingen. Cell lines used included human head and neck cancer cell lines Cal27, SCC-1, and SCC-25, and human monocytic cell line THP-1. All cell lines were tested free for Mycoplasma. Cell lines were authenticated with GenePrint10 (Promega) through JHH Genetic Resource Core Facility and stored in −70deg C in aliquots when not in use. Cells were cultured with RPMI-1640 medium, with 10% FCS, 10% L-glutamine, 10% Na-pyruvate, 10% Penicillin/Streptomycin and 0.1% beta-ME. All reagents were from Gibco®. When co-cultured with sorted MDSC, the FCS concentration was 1–2%. $CD14^+$ monocytes from healthy non-age matched volunteers were used for controls. Murine melanoma cell line B16, colon-cancer cell line CT26, and pancreatic cancer cell line Panc02 were obtained from ATCC. MOC1 murine head and neck cancer line was obtained from Ravi Uppaluri (Dana Farber).

MDSC isolation and flow cytometry analysis

Human MDSCs, characterized as $CD11b^+CD14^+HLA\text{-}DR^{low/-}$ were sorted from freshly obtained peripheral blood or tumor tissue from HNSCC patients undergoing surgical treatment at Johns Hopkins Hospital, Johns Hopkins Bayview Medical Center, or Vanderbilt University Medical Center. Peripheral blood mononuclear cells (PBMCs) were separated by Ficoll gradient prior to sorting with antibodies against human (h)CD11b, hCD14, and hHLA-DR conjugates, which were stained at 4°C for 30 minutes in dark at 1:50–200 dilution in 50μl FACS buffer prior to sorting or flow cytometry. Cells were sorted with a MoFlo MLS sorter (Beckman Coulter), as previously described (15). The purity of sorted

cells > 90%. All flow data were analyzed under Flowjo software. Human MDSCs were cultured in 2% FCS media.

Murine MDSCs, characterized as Gr-1^{+}CD11b^{+} or CD11b^{+}Ly6C^{high}, were sorted from splenocytes of 1–5 C57BL/6 mice (Jackson) whose tumor (B16, Panc02, MOC1) measured 0.125 cm^{3}. Splenocytes were harvested under sterile condition in RPMI culture media with 10% FCS, filtered with 40μm cell strainer, and RBC lysed with ACK buffer treated for 5 minutes. Fresh splenocytes were stained with antibodies under 4 °C in dark for 30min prior to sorting, and these MDSC were transferred intravenously as indicated in the *in vivo* tumor models below.

Proliferative index analysis

Sorted MDSCs were cultured in a 37°C incubator with 5% CO_2 in 1–2% FCS until use, Thawed tumor cell lines (human HNSCC cell lines-Cal27, SCC-1, SCC-25 [ATCC, Johns Hopkins Tissue Core] or murine cancer cell lines CT26 or B16) were passaged once, and they were pre-stained with cell proliferation dye eFlour450 (eBioscience) at a concentration of 5 μM at room temperature for 10 minutes and washed with PBS three times. Tumor cells and sorted MDSCs were cocultured in round-bottom 96-well plates for 3 days. 1–5×10^{5} MDSCs/well were typically used for these assays, with MDSC:tumor cell ratio ranging from 5:1 to 10:1. Stained tumor cells cocultured with peripheral monocytes from healthy individuals were used as controls at the same cell ratios.

Percentage of proliferating tumor cells was measured using the eFlour450 fluorescence signal detected by flow cytometry. Proliferative index was also measured using Ki67 staining of tumor cells. After co-incubation with MDSCs for 3–4 days, tumor cells were harvested and fixed with 5 mL 75% ethanol (added dropwise while vortexing) for 3 hours at −20°C, and the fixed tumor cells were stained with FITC-conjugated mouse anti-human Ki-67 (BD Pharmingen, room temperature, 30 minutes in dark). Immediately prior to flow cytometry analysis, 10 μL of propidium iodide (PI) staining solution was added to the cells to assess viability. Flow cytometry was used to analyze the stained cells.

Annexin V-FITC (ab14085; Abcam) staining to check for tumor cell apoptosis was assayed according to manufacturer's instructions. MDSCs' immunosuppression activity was assessed in control MDSCs that were not co-cultured with tumor cells at days 3–4 to ensure these cells were functionally T-cell immunosuppressive (see Supplementary Fig. S1). Briefly, matched CD4+ T-cells from the donors were stimulated with CD3/CD28 with or without sorted mMDSC from HNSCC patients. Either T-cell IFNγ production or CFSE dye dilutional assays were used to confirm the T-cell suppressive activity of mMDSC.

For cytokine incubation with eFlour450 stained Cal27 cells, we used the following concentrations – rhIL1b (500 pg/mL; R&D), IL18 (500 ng/mL; MBL Medical & Biological Lab), IL10 (5 ng/mL; R&D), IL6 (5 ng/mL), IL36 (50 ng/mL; R&D), IL33 (5 ng/mL; R&D), TGFβ (5 ng/mL; R&D), TNFα (100 pg/mL; R&D). 1×10^{5} Cal-27 cells were cultured in each well in 96-well-plate, flat bottom. 4–5 days after the incubation, cells were then collected to run flow cytometry for the proliferation index as described above.

Cytokine array

A Bio-Plex Pro Assays kit (Bio-Rad) was used to measure cytokines on the Bio-Plex system. The supernatant from sorted human MDSCs from peripheral blood or tumor tissue were collected 24 hours after the different treatment conditions. The assay was performed on a 96-well-plate. All samples, including standards, were assayed in duplicate or triplicate wells. Standard curve was generated using the Bio-Plex software, and all the values were within the effective detecting limits.

ELISA

200 μl of the supernatant from each well of cultured human MDSC under different treatments were collected at different time points for measurement of IL1β and IL18 using ELISA kits without dilutions (eBioscience, BMS618/2, MBL: 7620). 5×10^5 murine MDSCs were activated with 50–100 ng/mL of LPS (Calbiochem) for 24 hours. Each assay had duplicated wells for the standard curve and samples. Concentration was calculated from the standard curve using the recombinant cytokines, per the manufacturer's instructions.

Caspase-1 staining and inhibition

Fluorescent-labeled inhibitors of caspase-1 (FLICA) covalently bind to active caspase enzymes in cells. Caspase-1–specific FLICA 660 Assay kit (ImmunoChemistry) was used to stain the sorted human MDSCs at 37 °C for 1 hour, then washed 2 times with buffer provided in the kit, and counterstained with DAPI, per the assay protocol. FLICA stained cells (far red) were analyzed with a Hamamatsu Photonics C9100–02 EMCCD camera using the following filter set: Chroma #41137 – Excitation – HQ620/60; Chroma #39187 – Dichroic – Q660LP, and Chroma #40075 – Emission – HQ700/75. The objective used was an Olympus 40x NA 1.4, oil immersion. For caspase-1 inhibition, the caspase-1–specific inhibitor, Z-WEHD-FMK (BD Pharmingen ™), was added to cultured MDSCs at 80–100 μM for 24 hours (for cytokines analysis) or for 5 days (for cell proliferation assays).

Transwell system

HTS Transwell® 96-well plates with 1.0 μm polyester membranes were used to determine the effect of MDSCs on tumor cells without cell-cell contact. 10^5 sorted MDSCs were cultured in the upper chamber, with 10^5 eFluor450 stained SCC-25 or Cal27 tumor cells in the bottom chamber. Cell proliferative index was determined on day 4–6.

In vivo tumor model

Caspase-$1^{-/-}$ mice (Jackson Laboratory (B6N.129S2-Casp-1^{tm1flv} or NOD.129S2(B6)-Casp1tm1Sesh Casp4del/LtJ)) were housed in Johns Hopkins animal facility under institutional guidelines after animal IACUC protocol was approved. To generate chimeric mice, 5×10^6 bone marrow cells (BMC) from caspase$^{-/-}$ mice or wildtype C57BL/6 mice were adoptively transferred to lethally irradiated (10Gy) wildtype C57BL/6 mice. 8 weeks after bone marrow transfer, engraftment was confirmed by the presence of $CD45^+$ PBMCs. After engraftment confirmation, B16, MOC1, or Panc-02 tumor cells ($1–5\times10^5$/mouse) were subcutaneously injected into the chimeric mice. Tumors were measured daily or every 2 days with calipers, and mice were sacrificed when the tumors measured 2 cm in the largest

diameter. Depleting anti-CD3 (100 μg/mouse from InVivoMab, Lot number: 4773–2/0914 or clone 17A2 from Bio X Cell) were injected intraperitoneally twice a week in some cohorts. 2–5×10^6 isolated Gr-$1^+$$CD11b^+$ MDSCs (Miltenyi, Cat#130–094-538) harvested from the spleen of B16-or Panc02-bearing wildtype mice were injected intravenously into caspase-$1^{-/-}$ or wildtype mice with CD3 depletion on Day7, Day14 and Day21 after tumor injection. In some groups, splenic MDSCs were treated with racemic thalidomide (Sigma, Cat#1652500, 50 μg/mL) in RPMI supplemented with 10% FBS at 37°C, 5% CO_2 for 2–3 hours and then washed with PBS prior to adoptive transfer. Tumor sizes were measured with calipers daily, and tumor volumes were estimated using the formula V (cm^3) = 3.14 × [largest diameter × (perpendicular diameter)^2]/6.

SiRNA and qPCR

Pre-made inducible lentiviral particles suppressing the MyD88 gene (GenTarget Inc, #LVP 207) were used for siRNA targeting in Cal27 cells. Cal-27 cells at 65–70% confluency were transduced with lentiviral construct particles. The RFP reporter gene was used to sort transduced cells by flow cytometry. RFP^+ cells were labeled as Cal27-MyD88 KO cells after validation. Total RNA was extracted and reverse transcribed to cDNA with High Capacity RNA-to-cDNA kit (Applied Biosystems). Concentrations of cDNA were measured with Nanodrop 1000 (Thermo Scientific). A Taqman® gene expression assay that targets NFkB (Assay ID: Hs00765730_m1) was used to probe for NFκB expression in both the Cal27 and Cal27-MyD88 KO cells. The 18S rRNA was used as the internal control. 25 ng cDNA was used as the template, and 20μL reactions were carried out in 96-well plates using the Taqman Universal Master Mix II (2x) as the reaction cocktail. Double delta Ct (ΔΔCt method) analysis on NFkB transcripts was performed to provide its relative quantitation between the two cell lines (38). Assay was carried on the Applied Biosystems Veriti 9902 96-well thermal cycle PCR system. Thermal cycling parameters: 95°C for 10 minutes, denature at 95°C for 15seconds, and anneal/extend at 60°C for 1 minute, and then repeated for 40 cycles.

TCGA bioinformatics analysis

We compared RNA-Seq by Expectation Maximization (RSEM)-transformed caspase-1 gene expression with progression-free survival (Fig. 5A) and The Cancer Genome Atlas (TCGA)-defined subtype (Fig. 5B). The expression data was from the Broad Firehose (January 28th, 2016; https://gdac.broadinstitute.org/), and the survival and subtype data were retrieved from the TCGA Network (41); for each calculation, all samples with available data were used. The Cox proportional hazards ratio, 95% CI (confidence interval), and Wald *P* value were calculated using the *coxph* function from the R *Survival* package (Therneau, “A package for survival analysis in S,” Jan 1999), where patients were partitioned into two categories using a caspase-1 gene expression Z-score of 1.0 (i.e., patients with a Z-score <1.0 in one category, and patients with a Z-score ≥ in the second category; Fig. 5A). Significant association between caspase-1 gene expression and the basal vs. non-basal TCGA subtypes was calculated as the Wilcoxon rank-sum *P* value (Fig. 5B).

MDSC gene expression analysis by microarray

Sorted monocytic ($CD11b^+/HLA\text{-}DR^{low}/CD14^+$) and granulocytic (g)($CD11b^+/HLA\text{-}DR^{low}/CD15^+$ MDSC from peripheral blood of patients with advanced HNSCC as described (see above) were placed into Trizol (TRIzol®Reagent), and RNA isolation was done using the RNeasy Mini Kit (QIAGEN, www.qiagen.com). RNA quality was confirmed by analysis on the Agilient 2100 Bioanalyzer. Biotin-labeled targets were generated from 20 ng total human RNA using the NuGEN WT-Ovation Pico assay, as per the manufacturer's recommended protocols. Affymetrix Human Gene 1.0 ST microarrays (Affymetrix, Santa Clara, CA) were hybridized for 16 hours at 45° C with rotation (60rpm) as described in Affymetrix's GeneChip Expression Wash, Stain, and Scan User Manual (www.affymetrix.com). Fluorescent signals were determined using Affymetrix' GeneChip Scanner 3000 7G at default parameters described in the manufacturer's GeneChip Expression Analysis Technical Manual. Images were analyzed using the Affymetrix Command Console version 3 (AGCC v3.0), and processed into CEL files at the manufacturer's default settings. RMA normalized log2 signal values were extracted and summarized for gene-level analysis with the Partek Genomics Suite v6.6 (Partek Inc., St. Louis MO, USA). In some cases, the gene expression data for gMDSCs and mMDSCs were compared by one-way ANOVA using Partek, and the results were exported for examination and further evaluation to Spotfire DecisionSite (TIBCO Software Inc., Palo Alto CA, USA).

Statistics

The statistical analysis of the results was performed using Prism 6 software or Microsoft Excel v16 software. The ANOVA analysis was used to compare the differences among multiple groups. Two groups were compared using Fischer's exact test or student's t-test with a two-tailed distribution and calculated at 95% confidence. Differences were considered statistically significant at $P<0.05$. Kaplan-Meier curves were compared using the log-rank (Mantel Cox) test. When present, error bars reflect standard error of measurement (SEM).

Results

MDSCs with increased inflammasome complex can promote tumor cell proliferation

We sorted monocytic $CD11b^+CD14^+HLA\text{-}DR^{low/-}$ MDSCs (mMDSCs), from head and neck squamous cell cancer (HNSCC) patients, and demonstrated MDSC T-cell suppressive activity (Supplementary Fig. S1), and we assessed relative mRNA expression profiles for the MDSCs via microarray (15). We noted increased expression of inflammasome complex mRNAs that were correlated with increased IL1β and IL18 secretion (Fig. 1A and B). To characterize the functional significance of the inflammasome signaling in human mMDSCs, we modeled the human TME using cocultures of multiple HNSCC tumor cell lines (Cal27, SCC-1, SCC-25) with sorted mMDSCs to examine whether MDSCs can directly regulate the proliferation of tumor cells. When fluorescently labeled cancer cells were cocultured with mMDSCs without T cells, the proliferation index of the tumor cells was significantly enhanced in all HNSCC lines assayed without any changes in apoptosis (Fig. 1C, left panels; Supplementary Fig. S2). Most of the MDSCs sorted from the 21 HNSCC patients showed this ability to promote tumor cell proliferation, whereas monocytes from healthy donors did not alter tumor cell proliferation (Fig. 1C, right upper panel). The pro-tumorigenic MDSC

response was dependent on the ratio of MDSCs to tumor cells (Fig. 1C, lower right panel). MDSCs also increased the tumor cells' expression of Ki-67, a marker of cell proliferation, corroborating the dye dilutional assays (Fig. 1D).

To investigate whether the upregulated inflammasomes in MDSCs were related to their promotion of tumor cell proliferation, we treated human mMDSCs with the caspase-1–specific inhibitor, Z-WEHD-FMK, which reduced the secretion of IL1β and IL18 prior to the co-incubation assay (Fig. 2A). A caspase-1–specific FLICA assay was used independently to corroborate that caspase-1 was active *in situ* in the sorted human MDSCs (Fig. 2B). When the caspase-1 inhibitor, Z-WEHD-FMK, was added to the MDSCs prior to co-culture, we found that MDSCs decreased their ability to induce tumor cell proliferation (Fig. 2C).

Paracrine mitogenic activity is higher in monocytic MDSCs

When we compared the mitogenic induction between sorted gMDSCs ($CD15^+CD14^-$ $HLA\text{-}DR^{low/-}$) to the mMDSCs from the same patients, we noted that mMDSCs had greater ability to promote tumor proliferation (Fig. 3A). When we compared the relative expression profiles between mMDSCs and gMDSCs, mMDSCs had greater expression of inflammasome complex mRNAs than gMDSCs (Fig. 3B). We reasoned that if the promotion of tumor proliferation is dependent on caspase-1/IL1β/IL18 signaling pathway, this phenotype would be a paracrine-dependent mechanism, and cell-cell contact would not be necessary. We performed the tumor proliferation assay in a transwell assay, and we noted that the presence of mMDSCs in the test chamber increased the proliferation index of tumor cells in the other chamber (Fig. 3C, $P<0.001$). We also showed that supernatants from human mMDSCs phenocopied the enhanced proliferative index of HNSCC cells co-incubated with MDSCs (Fig. 3D, right panel). When we followed the proliferative index of Cal27 with the incubation of recombinant human cytokines expressed by MDSCs, enhanced proliferation was noted when IL1β, IL18, IL6, and IL10 were combined, whereas IL1β and IL18 individually only had about 1.3 fold effect (Supplementary Fig. S3).

Myeloid caspase-1 directly promotes carcinogenesis

Because the *in vitro* cell mixing experiments do not replicate the complexity of the TME, we directed our attention towards *in vivo* characterization of myeloid caspase-1, in the context of a syngeneic tumor model. In order to probe whether MDSC caspase-1 can directly promote tumor proliferation *in vivo*, we used chimeric C57BL/6 mice adoptively transferred with bone marrow cells (BMCs) from caspase-1 null or wildtype control mice. We initially showed that murine $Gr1^+CD11b^+$ MDSCs expressed IL1β and IL18 (Supplementary Fig. S4), and its coculture with B16 or CT26 tumor cells promoted caspase-1–dependent tumor cell proliferation as we observed with human mMDSCs (Fig. 4A). In chimeric mice with caspase-1 null hematopoietic cells, B16 tumor growth was significantly blunted, regardless of whether $CD3^+$ T cells were depleted or not (Fig. 4B, left upper panel). The T cell–independent effect of caspase-1 signaling was more prominent in this subcutaneous tumor injection model. We repeated the experiment with Panc02 pancreatic cancer cells (Fig 4B, right upper panel), as well as MOC1 oral cavity tumor cells (Supplementary Fig. S5) with the same results. When wildtype $Gr1^+CD11b^+$ MDSCs harvested from B16-bearing

mice were adoptively transferred into caspase-1 null chimeric mice after tumor injection, the protective effect of absent caspase-1 signaling was reversed (Fig. 4B, left lower panel). To test whether pharmacologic blockade of MDSC inflammasome signaling can specifically phenocopy the caspase-1 null chimeric mice, we treated wildtype MDSCs with caspase-1 inhibiting thalidomide prior to their adoptive transfer into tumor-bearing mice that had caspase-1 deficiency and T cells depletion (40). Although the wildtype MDSCs restored their pro-tumorigenic effect, thalidomide-treated MDSCs failed to increase the pro-tumorigenic tumor growth rate of B16 in chimeric mice (Fig. 4B, lower right panel). Together these results show that caspase-1 activity in MDSCs could directly promote *in vivo* tumor growth, independent of T cells.

Caspase-1 expression in the TME correlates with worse prognosis

To investigate the role of caspase-1 as a potential prognostic marker in HNSCC patients, we correlated caspase-1 gene expression with survival and subtype using data from a TCGA HNSCC patient cohort (Fig. 5)(41). Elevated caspase-1 expression was significantly associated with decreasing progression-free survival in TCGA HNSCC patients (Fig 5A). Similarly, when we probed for caspase-1 expression in the basal subtype, which has previously been associated with worse clinical outcomes with relative absence of T-cell infiltration (39, 42), caspase-1 expression was significantly higher in the basal subtype than in the non-basal subtypes (Fig. 5B).

MDSCs' promotion of tumor proliferation is dependent on tumor cell MyD88 signaling

Because both IL1β and IL18 signaling results in activation of tumor MyD88 signaling pathway to induce oncogenic transcription factors NFkB and AP-1 (27, 43), we inquired whether MDSCs' stimulation of MyD88 signaling is partly responsible for the enhanced mitogenic signaling in HNSCC cells. We suppressed the MyD88 gene expression in Cal27 HNSCC cell line with siRNA that also expressed an RFP reporter gene, and we sorted the RFP-expressing Cal27 cells. MyD88 knockdown in Cal27 cells showed significantly lower NFkB transcripts as indicated by the higher number of NFkB qPCR cycling. (Fig. 6A). When we compared the proliferation index of wildtype Cal27 cells and the MyD88 suppressed Cal27 cells cocultured with MDSCs, the MDSC-dependent promotion of tumor cell proliferation was significantly blunted in the MyD88-suppressed tumor cells *in vitro* (Fig. 6B). We reasoned, therefore, that tumor cells deficient in MyD88 signaling would not be affected by myeloid caspase-1 signaling *in vivo*. Thus, we compared the tumor growth rate of B16 cells and B16 MyD88 knockdown cells in wildtype mice and found that MyD88 suppression significantly decreased the growth rate of B16 *in vivo* (Fig. 6C). However, using chimeric mice adoptively transferred with caspase-1 null BMCs under T cell–depleting conditions, MyD88 signaling in the B16 tumor cells resulted in no differential tumor growth rate *in vivo* compared to control tumor cells with transduction of scrambled shRNA (Fig 6C). The blunted tumor growth rates attributable to myeloid caspase-1 signaling seen previously in Fig. 4 were not found in these tumors cells lacking MyD88/NFkB oncogenic signals.

Discussion

Depending on the preclinical models used, the role of the inflammasome in carcinogenesis has been contradictory and context-dependent (27, 35). In one colorectal metastasis model, the inflammasome complex was found to suppress metastasis via NK cell activity (44), and others showed that NLRP3 signaling in hematopoietic compartment can be protective against tumorigenesis through bone marrow chimera studies (31, 33). In other models, however, NLRP3 null mice had reduced lung metastasis with B16-F10 tumor cells (45). These examples highlight the complex association between the inflammasome complex and cancer, which were have been reviewed in detail (46–48). How these various context-dependent mechanisms of the inflammasome complex in murine models are pertinent to human cancer biology is still unclear. Hence, clinical development of inflammasome targeting agents have been somewhat hindered by these conflicting preclinical murine results. However, an intriguing correlative finding was noted in atherosclerotic patients treated with canakinumab (blocks IL1β) (49, 50). Although canakinumab effectively reduced myeloid dependent atherosclerotic disease, the treated group also showed surprising reduction in lung cancer incidence and cancer-associated mortality. Combined with our findings, translational development of IL1β or inflammasome blocking agents in human malignancies is warranted.

Although the TME is infiltrated with both lymphocytic and myeloid cells, there are a subset of aggressive carcinomas that are T-cell poor and may be amenable for MDSC targeting (21). Interestingly, these “non-inflamed” tumors have been reported to be less responsive to checkpoint inhibitors, and the ability to inhibit pro-tumorigenic myeloid cells will be an important clinical strategy going forward in immune-oncology (51). Our previous report in preclinical MOC head & neck tumor model with higher MDSC tumor infiltration relative to tumor-infiltrating lymphocytes were more responsive to immune checkpoint inhibition with the addition of MDSC depleting antibody (52). Rilonacept and canakinumab are two examples of IL1β targeting agents that are safe in early clinical trials for chronic inflammatory diseases, so clear clinical pathways to translate inflammasome targeting agents into immune-oncological trials exist (48, 52). Our demonstration that MDSC caspase-1 directly promoted NFkB-dependent tumor proliferation also offers potential biomarker correlative analysis on the tumor intrinsic MyD88/ NFkB signaling that may be associated with clinical response with these anti-inflammasome agents.

With regards to clinical development, several clinical trials that target myeloid chemokine receptors (www.clinicaltrials.gov) are underway. Although our findings cannot answer how to best target MDSCs, pharmacologic use of inflammasome blocking agents, as shown by our experiments with thalidomide, are supported by our data. The potential problem with chemokine receptor blocking strategies is that different types of MDSCs and other immunosuppressive myeloid cells may have differential recruitment pathways. We previously showed that CXCR2 may be responsible for granulocytic MDSC recruitment, whereas CSF1R primarily recruits monocytic MDSC (52). Others have shown that IL1β from epithelial cell can recruit MDSCs into the tumor (45). We, therefore, support a global pharmacologic targeting of the inflammasome pathway in tumor cells, as well as myeloid cells, to potentially induce greater antitumor responses.

For the downstream mechanism of action of caspase-1 in the TME, the literature points to discordant effects of IL1β and IL18, the two primary downstream cytokines from caspase-1 activation. In our limited cytokine-Cal27 incubation experiments, a significant tumorigenic response to these cytokines, primarily when the cytokines were combined, was seen. In general, IL1β has been linked to a tumor induction and progression, whereas IL18 has been associated with NK cell-dependent protection against tumors (43, 53–55). From our adoptive transfer experiments with caspase-1 null mice, we hypothesize that other caspase-1 dependent secretome factors or IL1β may prevail over the potential protective impact of IL18 induction of NK cells in the TME. There are potentially other mechanisms that may explain our *in vivo* data, such as caspase-1's promotion of tumor proliferation may be one of many T cell–independent mechanism of carcinogenesis. The dramatic antitumor effect in our chimeric mice suggests that other downstream effectors of inflammasome complex, such as pyroptosis, may also regulate the TME. Our findings offer an avenue of research assessing downstream effectors of myeloid inflammasomes that can shape both the primary tumor and the premetastatic niche in both the draining lymph nodes and distant organ sites (26).

Although we focused on caspase-1 in MDSCs, their activity on macrophages and other myeloid cells that infiltrate the tumor will require further investigation. Given the plasticity of MDSCs in the TME and their tendency to differentiate *ex vivo*, the ability to differentiate tumor-associated MDSCs from other myeloid cells may be difficult. Although early reports show that immature $VEGF^{+}$ myeloid cells may help establish the premetastatic niche and the discoveries that STAT3 in myeloid cells can promote metastasis (56, 57), tumor-infiltrating myeloid cells, such as MDSCs, may become an important regulator of metastasis. These previously reported links between MDSCs and metastasis may explain how myeloid caspase-1 signaling is associated with overall survival in the TCGA database. Although most of these works have focused on how these immunosuppressive myeloid cells regulate the intermediary immune cells to render cancer more metastatic, we presented evidence in the human system that MDSCs could have a direct mitogenic response, which may be relevant in the context of the premetastatic niche. Such a direct pro-carcinogenic mechanism has been advanced in murine models of lung metastasis, which shows MDSCs may promote epithelial-mesenchymal transition (26). Although our *in vitro* system did not account for T cells, NK cells, and stromal cells in the TME, we argue that the immunosuppressive mechanism of MDSCs in the TME must also account for the basal oncogenic signals that MDSCs can provide for the tumor cells. Lastly, our report further supports the need to redefine the functional definition of MDSCs (58).

Supplementary Material

Refer to Web version on PubMed Central for supplementary material.

Acknowledgements

We like to acknowledge Dr. Ravi Uppaluri (Dana Farber Cancer Center) for providing the MOC1 HNSCC cell lines. We also like to thank Conover Talbot Jr (Johns Hopkins School of Medicine) for the bioinformatics analysis of the microarray.

Funding Support: The authors thank the NIH for support of this research (NIH R01CA178613). The authors also thank the Bloomberg-Kimmel Institute for Cancer Immunotherapy and the Baker family for support.

References

1. Gabrilovich DI, Bronte V, Chen SH, Colombo MP, Ochoa A, Ostrand-Rosenberg S, et al. The terminology issue for myeloid-derived suppressor cells. Cancer Res. 2007;67:425; author reply 426. [PubMed: 17210725]
2. Gabrilovich DI, Nagaraj S. Myeloid-derived suppressor cells as regulators of the immune system. Nat Rev Immunol. 2009;9:162–74. [PubMed: 19197294]
3. Rodriguez PC, Ochoa AC. Arginine regulation by myeloid derived suppressor cells and tolerance in cancer: mechanisms and therapeutic perspectives. Immunol Rev. 2008;222:180–91. [PubMed: 18364002]
4. Talmadge JE. Pathways mediating the expansion and immunosuppressive activity of myeloid-derived suppressor cells and their relevance to cancer therapy. Clin Cancer Res. 2007;13:5243–8. [PubMed: 17875751]
5. Ostrand-Rosenberg S, Sinha P. Myeloid-derived suppressor cells: linking inflammation and cancer. J Immunol. 2009;182:4499–506. [PubMed: 19342621]
6. Marigo I, Dolcetti L, Serafini P, Zanovello P, Bronte V. Tumor-induced tolerance and immune suppression by myeloid derived suppressor cells. Immunol Rev. 2008;222:162–79. [PubMed: 18364001]
7. Marvel D, Gabrilovich DI. Myeloid-derived suppressor cells in the tumor microenvironment: expect the unexpected. J Clin Invest. 2015:1–9. [PubMed: 25654544]
8. Yang L, Huang J, Ren X, Gorska AE, Chytil A, Aakre M, et al. Abrogation of TGF beta signaling in mammary carcinomas recruits Gr-1+CD11b+ myeloid cells that promote metastasis. Cancer Cell. 2008;13:23–35. [PubMed: 18167337]
9. Johnston PA, Grandis JR. STAT3 SIGNALING: Anticancer Strategies and Challenges. Mol Interv. 2011;11:18–26. [PubMed: 21441118]
10. Shojaei F, Wu X, Qu X, Kowanetz M, Yu L, Tan M, et al. G-CSF-initiated myeloid cell mobilization and angiogenesis mediate tumor refractoriness to anti-VEGF therapy in mouse models. Proc Natl Acad Sci U S A. 2009;106:6742–7. [PubMed: 19346489]
11. Erler JT, Bennewith KL, Cox TR, Lang G, Bird D, Koong A, et al. Hypoxia-induced lysyl oxidase is a critical mediator of bone marrow cell recruitment to form the premetastatic niche. Cancer Cell. 2009;15:35–44. [PubMed: 19111879]
12. Gabrilovich DI, Ostrand-Rosenberg S, Bronte V. Coordinated regulation of myeloid cells by tumours. Nat Rev Immunol. 2012;12:253–68. [PubMed: 22437938]
13. Elinav E, Nowarski R, Thaiss CA, Hu B, Jin C, Flavell RA. Inflammation-induced cancer: crosstalk between tumours, immune cells and microorganisms. Nat Rev Cancer. 2013;13:759–71. [PubMed: 24154716]
14. Coussens LM, Werb Z. Inflammation and cancer. Nature. 2002;420:860–7. [PubMed: 12490959]
15. Vasquez-Dunddel D, Pan F, Zeng Q, Gorbounov M, Albesiano E, Fu J, et al. STAT3 regulates arginase-I in myeloid-derived suppressor cells from cancer patients. J Clin Invest. 2013;123:1580–9. [PubMed: 23454751]
16. Grivennikov S, Karin E, Terzic J, Mucida D, Yu GY, Vallabhapurapu S, et al. IL-6 and Stat3 are required for survival of intestinal epithelial cells and development of colitis-associated cancer. Cancer Cell. 2009;15:103–13. [PubMed: 19185845]
17. Bromberg J, Wang TC. Inflammation and cancer: IL-6 and STAT3 complete the link. Cancer Cell. 2009;15:79–80. [PubMed: 19185839]
18. Quante M, Bhagat G, Abrams JA, Marache F, Good P, Lee MD, et al. Bile acid and inflammation activate gastric cardia stem cells in a mouse model of Barrett-like metaplasia. Cancer Cell. 2012;21:36–51. [PubMed: 22264787]
19. Takai A, Toyoshima T, Uemura M, Kitawaki Y, Marusawa H, Hiai H, et al. A novel mouse model of hepatocarcinogenesis triggered by AID causing deleterious p53 mutations. Oncogene. 2009;28:469–78. [PubMed: 18997814]

20. Zitvogel L, Kepp O, Galluzzi L, Kroemer G. Inflammasomes in carcinogenesis and anticancer immune responses. Nat Immunol. 2012;13:343–51. [PubMed: 22430787]
21. Spranger S, Spaapen RM, Zha Y, Williams J, Meng Y, Ha TT, et al. Up-Regulation of PD-L1, IDO, and Tregs in the Melanoma Tumor Microenvironment Is Driven by CD8+ T Cells. Sci Transl Med. 2013;5:200ra116.
22. Gibney GT, Weiner LM, Atkins MB. Predictive biomarkers for checkpoint inhibitor-based immunotherapy. Lancet Oncol. 2016;17:e542–51. [PubMed: 27924752]
23. Tsujikawa T, Kumar S, Borkar RN, Azimi V, Thibault G, Chang YH, et al. Quantitative Multiplex Immunohistochemistry Reveals Myeloid-Inflamed Tumor-Immune Complexity Associated with Poor Prognosis. Cell Rep. 2017;19:203–17. [PubMed: 28380359]
24. Califano JA, Khan Z, Noonan KA, Rudraraju L, Zhang Z, Wang H, et al. Tadalafil augments tumor specific immunity in patients with head and neck squamous cell carcinoma. Clin Cancer Res. 2015;21:30–8. [PubMed: 25564570]
25. Ko JS, Zea AH, Rini BI, Ireland JL, Elson P, Cohen P, et al. Sunitinib mediates reversal of myeloid-derived suppressor cell accumulation in renal cell carcinoma patients. Clin Cancer Res. 2009;15:2148–57. [PubMed: 19276286]
26. Ouzounova M, Lee E, Piranlioglu R, El Andaloussi A, Kolhe R, Demirci MF, et al. Monocytic and granulocytic myeloid derived suppressor cells differentially regulate spatiotemporal tumour plasticity during metastatic cascade. Nat Commun. 2017;8:14979. [PubMed: 28382931]
27. Rakoff-Nahoum S, Medzhitov R. Regulation of spontaneous intestinal tumorigenesis through the adaptor protein MyD88. Science. 2007;317:124–7. [PubMed: 17615359]
28. Salcedo R, Worschech A, Cardone M, Jones Y, Gyulai Z, Dai RM, et al. MyD88-mediated signaling prevents development of adenocarcinomas of the colon: role of interleukin 18. J Exp Med. 2010;207:1625–36. [PubMed: 20624890]
29. Elinav E, Henao-Mejia J, Flavell RA. Integrative inflammasome activity in the regulation of intestinal mucosal immune responses. Mucosal Immunol. 2013;6:4–13. [PubMed: 23212196]
30. Hu B, Elinav E, Huber S, Booth CJ, Strowig T, Jin C, et al. Inflammation-induced tumorigenesis in the colon is regulated by caspase-1 and NLRC4. Proc Natl Acad Sci U S A. 2010;107:21635–40. [PubMed: 21118981]
31. Zaki MH, Vogel P, Body-Malapel M, Lamkanfi M, Kanneganti TD. IL-18 production downstream of the Nlrp3 inflammasome confers protection against colorectal tumor formation. J Immunol. 2010;185:4912–20. [PubMed: 20855874]
32. Normand S, Delanoye-Crespin A, Bressenot A, Huot L, Grandjean T, Peyrin-Biroulet L, et al. Nod-like receptor pyrin domain-containing protein 6 (NLRP6) controls epithelial self-renewal and colorectal carcinogenesis upon injury. Proc Natl Acad Sci U S A. 2011;108:9601–6. [PubMed: 21593405]
33. Allen IC, TeKippe EM, Woodford RM, Uronis JM, Holl EK, Rogers AB, et al. The NLRP3 inflammasome functions as a negative regulator of tumorigenesis during colitis-associated cancer. J Exp Med. 2010;207:1045–56. [PubMed: 20385749]
34. Zaki MH, Boyd KL, Vogel P, Kastan MB, Lamkanfi M, Kanneganti TD. The NLRP3 inflammasome protects against loss of epithelial integrity and mortality during experimental colitis. Immunity. 2010;32:379–91. [PubMed: 20303296]
35. Fabbi M, Carbotti G, Ferrini S. Context-dependent role of IL-18 in cancer biology and counter-regulation by IL-18BP. J Leukoc Biol. 2015;97:665–75. [PubMed: 25548255]
36. Malik A, Sharma D, Zhu Q, Karki R, Guy CS, Vogel P, et al. IL-33 regulates the IgA-microbiota axis to restrain IL-1alpha-dependent colitis and tumorigenesis. J Clin Invest. 2016;126:4469–81. [PubMed: 27775548]
37. Bruchard M, Mignot G, Derangere V, Chalmin F, Chevriaux A, Vegran F, et al. Chemotherapy-triggered cathepsin B release in myeloid-derived suppressor cells activates the Nlrp3 inflammasome and promotes tumor growth. Nat Med. 2013;19:57–64. [PubMed: 23202296]
38. Rao X, Huang X, Zhou Z, Lin X. An improvement of the 2^(-delta delta CT) method for quantitative real-time polymerase chain reaction data analysis. Biostat Bioinforma Biomath. 2013;3:71–85. [PubMed: 25558171]

39. Keck MK, Zuo Z, Khattri A, Stricker TP, Brown CD, Imanguli M, et al. Integrative analysis of head and neck cancer identifies two biologically distinct HPV and three non-HPV subtypes. Clin Cancer Res. 2015;21:870–81. [PubMed: 25492084]
40. Keller M, Sollberger G, Beer HD. Thalidomide inhibits activation of caspase-1. J Immunol. 2009;183:5593–9. [PubMed: 19843943]
41. Cancer Genome Atlas Network. Comprehensive genomic characterization of head and neck squamous cell carcinomas. Nature. 2015;517:576–82. [PubMed: 25631445]
42. Chung CH, Parker JS, Karaca G, Wu J, Funkhouser WK, Moore D, et al. Molecular classification of head and neck squamous cell carcinomas using patterns of gene expression. Cancer Cell. 2004;5:489–500. [PubMed: 15144956]
43. Zhao X, Rong L, Zhao X, Li X, Liu X, Deng J, et al. TNF signaling drives myeloid-derived suppressor cell accumulation. J Clin Invest. 2012;122:4094–104. [PubMed: 23064360]
44. Dupaul-Chicoine J, Arabzadeh A, Dagenais M, Douglas T, Champagne C, Morizot A, et al. The Nlrp3 Inflammasome Suppresses Colorectal Cancer Metastatic Growth in the Liver by Promoting Natural Killer Cell Tumoricidal Activity. Immunity. 2015;43:751–63. [PubMed: 26384545]
45. Chow MT, Sceneay J, Paget C, Wong CS, Duret H, Tschopp J, et al. NLRP3 suppresses NK cell-mediated responses to carcinogen-induced tumors and metastases. Cancer Res. 2012;72:5721–32. [PubMed: 22986739]
46. Petrilli V The multifaceted roles of inflammasome proteins in cancer. Curr Opin Oncol. 2017;29:35–40. [PubMed: 27875342]
47. Karki R, Man SM, Kanneganti TD. Inflammasomes and Cancer. Cancer Immunol Res. 2017;5:94–9. [PubMed: 28093447]
48. Jha S, Brickey WJ, Ting JP. Inflammasomes in Myeloid Cells: Warriors Within. Microbiol Spectr. 2017;5:10.1128/microbiolspec.MCHD,0049-2016.
49. Ridker PM, MacFadyen JG, Thuren T, Everett BM, Libby P, Glynn RJ, et al. Effect of interleukin-1beta inhibition with canakinumab on incident lung cancer in patients with atherosclerosis: exploratory results from a randomised, double-blind, placebo-controlled trial. Lancet. 2017.
50. Ridker PM, Everett BM, Thuren T, MacFadyen JG, Chang WH, Ballantyne C, et al. Antiinflammatory Therapy with Canakinumab for Atherosclerotic Disease. N Engl J Med. 2017.
51. Tobin RP, Davis D, Jordan KR, McCarter MD. The clinical evidence for targeting human myeloid-derived suppressor cells in cancer patients. J Leukoc Biol. 2017;102:381–91. [PubMed: 28179538]
52. Clavijo PE, Moore EC, Chen J, Davis RJ, Friedman J, Kim YJ et al. Oncotarget. 2017; 8:55804–55820. [PubMed: 28915554]
53. Carmi Y, Dotan S, Rider P, Kaplanov I, White MR, Baron R, et al. The role of IL-1beta in the early tumor cell-induced angiogenic response. J Immunol. 2013;190:3500–9. [PubMed: 23475218]
54. Tarassishin L, Casper D, Lee SC. Aberrant expression of interleukin-1beta and inflammasome activation in human malignant gliomas. PLoS One. 2014;9:e103432.
55. Tu S, Bhagat G, Cui G, Takaishi S, Kurt-Jones EA, Rickman B, et al. Overexpression of interleukin-1beta induces gastric inflammation and cancer and mobilizes myeloid-derived suppressor cells in mice. Cancer Cell. 2008;14:408–19. [PubMed: 18977329]
56. Kaplan RN, Riba RD, Zacharoulis S, Bramley AH, Vincent L, Costa C, et al. VEGFR1-positive haematopoietic bone marrow progenitors initiate the pre-metastatic niche. Nature. 2005;438:820–7. [PubMed: 16341007]
57. Deng J, Liu Y, Lee H, Herrmann A, Zhang W, Zhang C, et al. S1PR1-STAT3 signaling is crucial for myeloid cell colonization at future metastatic sites. Cancer Cell. 2012;21:642–54. [PubMed: 22624714]
58. Bronte V, Brandau S, Chen SH, Colombo MP, Frey AB, Greten TF, et al. Recommendations for myeloid-derived suppressor cell nomenclature and characterization standards. Nat Commun. 2016;7:12150. [PubMed: 27381735]

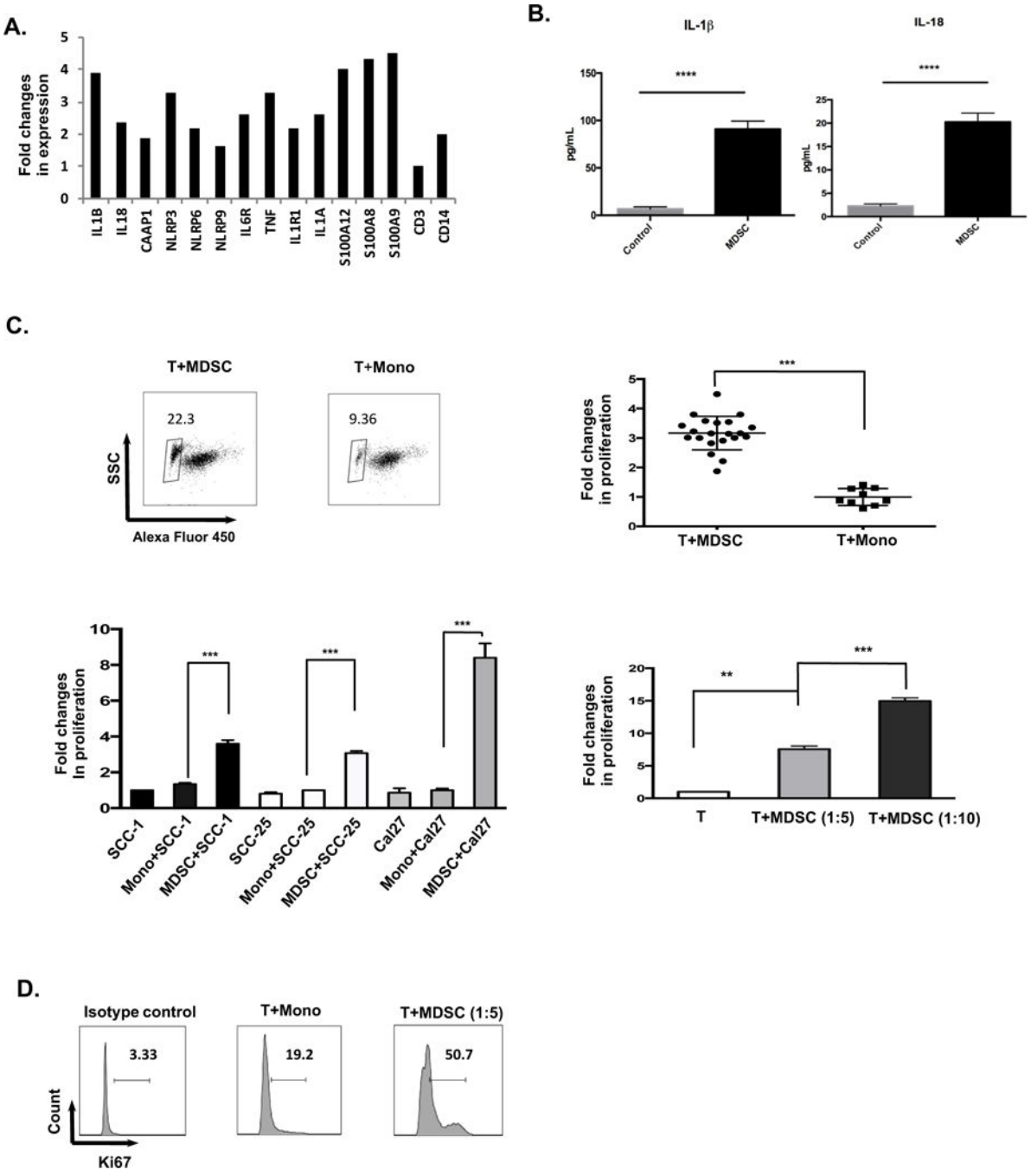

Figure 1. Inflammasome complex expression is increased in human MDSCs and can directly increase proliferation of tumor cells in vitro.

(A) Relative mRNA expression profile of inflammasome complex genes via an MDSC microarray. CD3 transcript expression was used as the relative negative control to generate folds changes (listed on the y-axis). (B) Secretion of IL1β and IL18 from sorted human MDSCs using Bio-Plex. Control: culture media only. (C) Sorted MDSCs from HNSCC patients and $CD14^{+}CD11b^{+}$ monocytes from healthy donors (controls) were cocultured with HNSCC cancer cell lines (T) – SSC-1, SCC-25, Cal27 – prelabeled with cell proliferation dye eFluor 450. Dye-dilutional shifts of live tumor cells were used to quantitate fold

change of proliferating cells. Upper left panel: Representative plot showing proliferation of tumor cells with MDSCs or control monocytes. Lower left panel: Summarizes proliferation changes for 3 HNSCC cell lines. Upper right panel: Proliferation changes of sorted mMDSCs ($CD14^+CD11b^+HLA\text{-}DR^{lo}$) from advanced HNSCC patients (N=21, error bars are the SEM of fold changes from each biospecimens) or control monocytes cocultured with Cal27 cells. Lower right panel: Different ratios of cancer cells to MDSCs were used to show dose-response effect on tumor proliferation. Cal27:MDSC = 1:5 or 1:10. T = Cal27 only. (D) Expression of Ki67 was analyzed by flow cytometry in tumor cells after incubation with MDSCs or control monocytes. Histograms represent Ki67 expression in different groups. T: MDSC=1:5. Control groups: isotype control antibody and control monocytes from healthy individuals. $^{**}P<0.01$, $^{***}P<0.001$. Each of the *in vitro* experiments were repeated at least 3 times independently. Error bars in panels B represent SEM from triplicates.

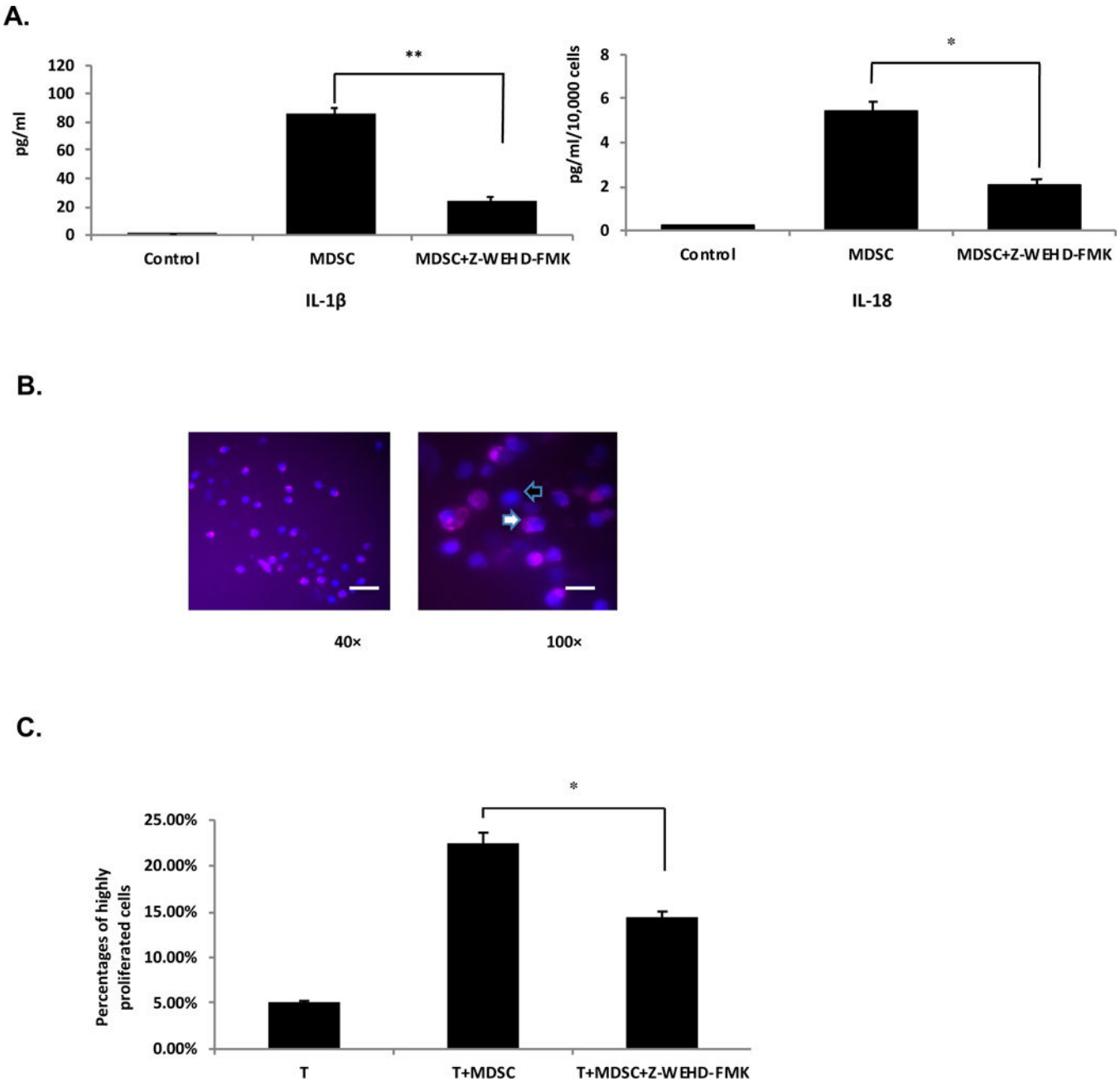

Figure 2. Inhibition of caspase-1 activity reduces MDSCs' ability to promote carcinogenesis.

(A) IL1β and IL18 production (ELISA) by sorted HNSCC patient mMDSCs ($CD14^+CD11b^+HLA\text{-}DR^{lo}$) with and without inhibition of caspase-1 using Z-WEHD-FMK. $^{**}P<0.01$, $^{*}P<0.05$. Control: monocytes from healthy individuals without inhibitor. Bar graphs are representative of at least 3 repeats of experiments with duplicate wells. (B) FLICA (Fluorescent labeled inhibitor of Caspase-1), covalently binds to active caspase-1, was used to visualize caspase-1 activity in mMDSCs. Nuclei were counter-stained with DAPI (black arrow). Caspase-1 staining is far-red FLICA fluorescence (white arrow). Pictures shown in 40x and 100x magnifications. Scale bar represent 100 μm in 40x, and 250μm in 100x. (C) Proliferation (%) of Cal27 with and without Z-WEHD-FMK. Control

group: Cal27 cultured with monocytes from healthy individuals. *$P<0.05$. Each of the *in vitro* experiments were repeated at least 3 times independently. Error bars in panels A and C represent SEM from triplicates.

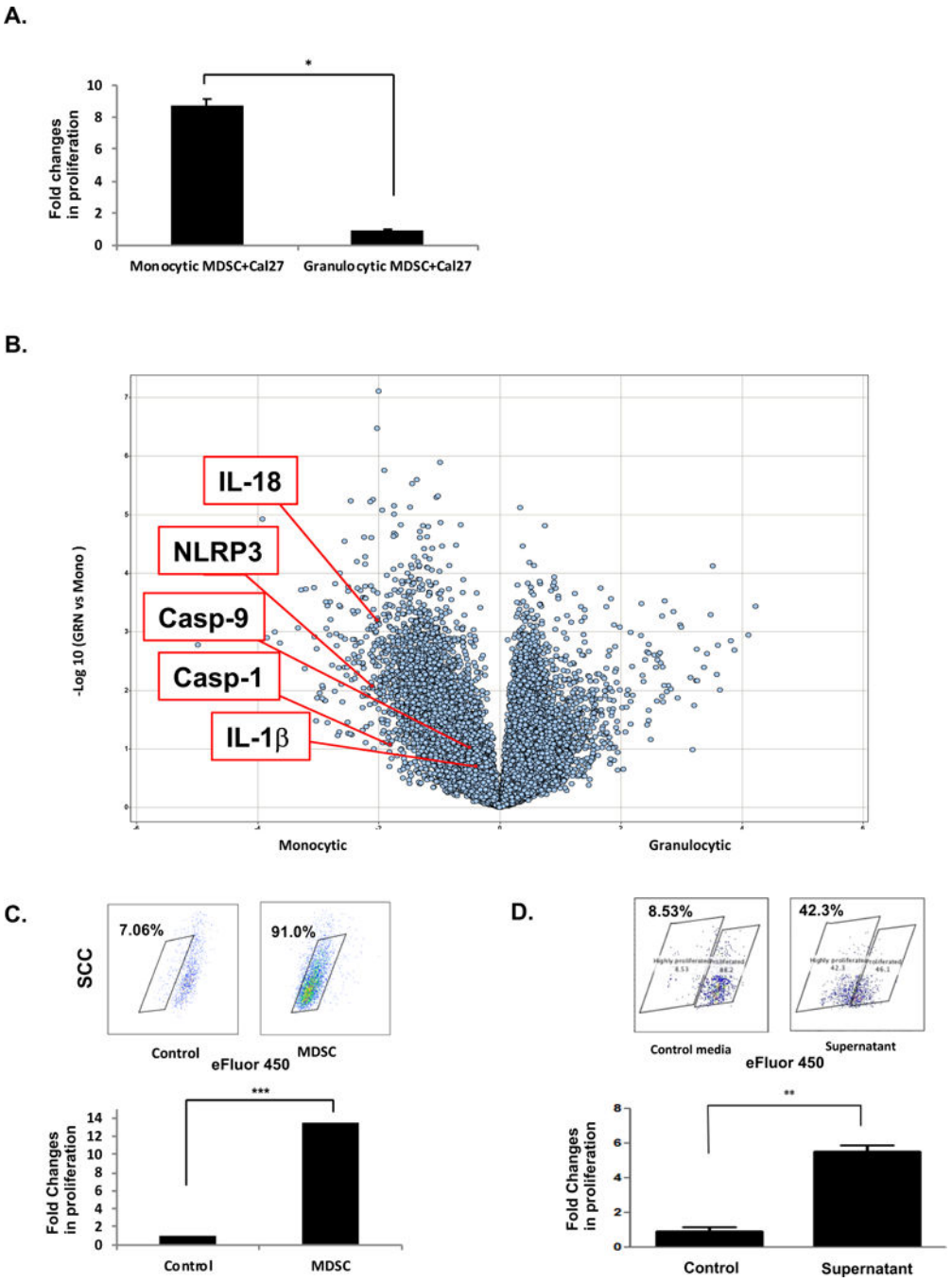

Figure 3. MDSCs' promotion of tumor proliferation is differentially enhanced in monocytic MDSCs and granulocytic MDSCs and is not dependent on cell-cell contact.

(A) Matched monocytic MDSCs were compared to granulocytic MDSCs ($CD15^{+}CD14^{-}$ $HLA\text{-}DR^{-}$) in their ability to promote tumor proliferation. Assays were replicated 5 times, and a representative result is displayed. *P<0.05. (B) Volcano plot of the differential microarray analysis of inflammasome complex genes between mMDSCs and gMDSCs. (C) Transwell assay to assess whether cell-cell contact was required for proliferation promotion. Transwell upper chamber: Sorted human MDSCs: Transwell bottom chamber: Seeded eFluor405-stained Cal27 cells. Fresh RPMI plus 2% serum without MDSCs were used as

controls (in the upper chamber). Proliferative index was determined by dye dilutional assay using flow cytometry. Representative plot also shown (top). ***P<0.001. (D) Supernatant from mMDSCs were added to eFluor405-stained SCC-1 cells, and the proliferative index was determined as noted above. Fresh RPMI (with 2% serum) with monocytes from healthy individuals was used as controls. Dot plots (upper panel) represent the dye dilutional analysis, and the bar graph (lower panel) shows the fold changes of tumor proliferation. **P<0.01. Each of the *in vitro* experiments were repeated at least 3 times independently. Error bars in panels A, C, and D represent SEM from triplicates.

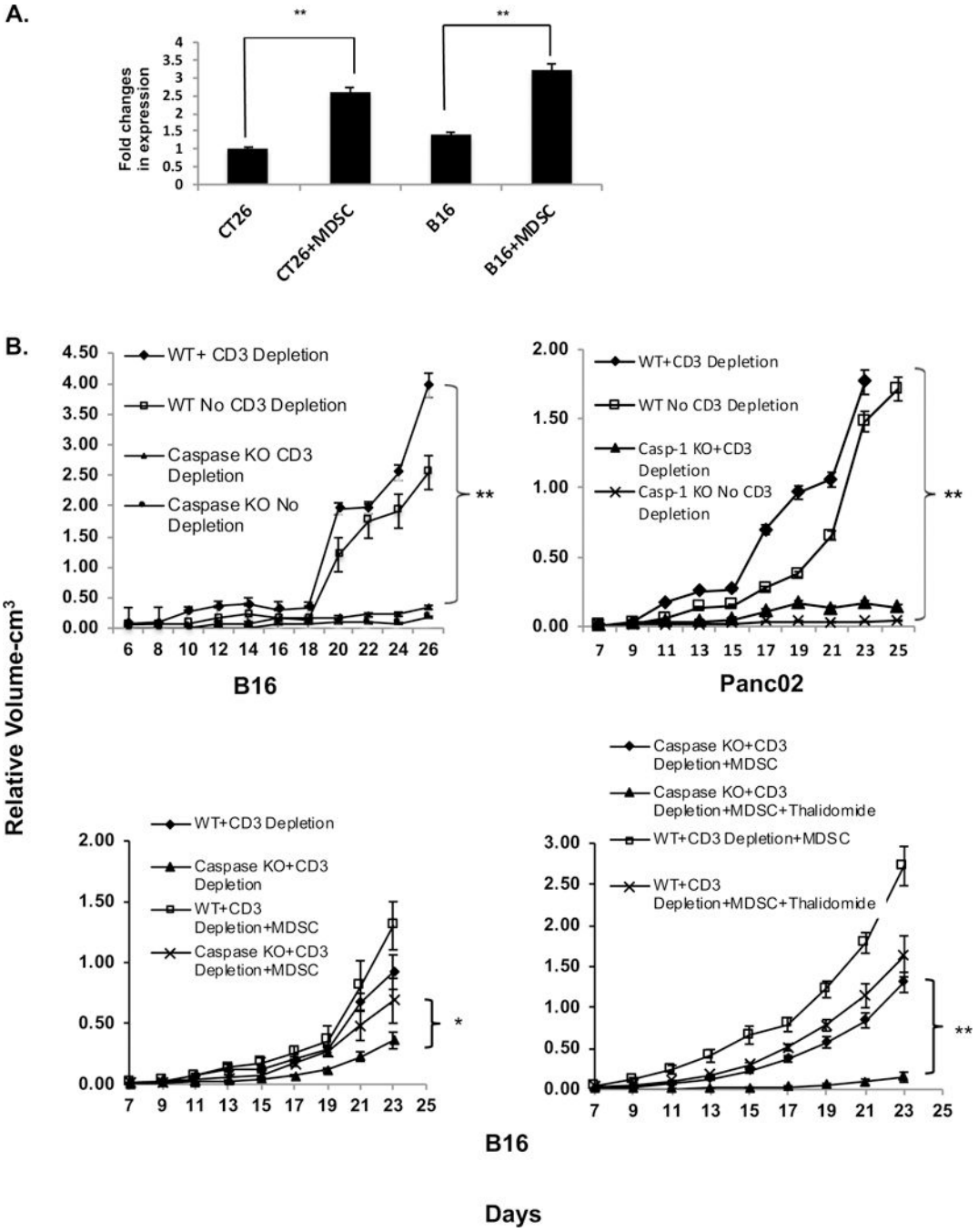

Figure 4. MDSC caspase-1 directly promotes carcinogenesis.

(A) Murine $Gr1^{+}CD11b^{+}$ MDSCs (produced IL1β and IL18, Supplementary Fig. S3) were cocultured with CT26 and B16 cells (pre-stained with eFluor450), and the fluorescence dilution of tumor cells were analyzed. Each experiment was performed in triplicate and repeated 3 times. (B) Tumor growth experiments *in vivo* were performed with chimeric C57BL/6 mice adoptively transferred with bone marrow cells (BMCs) from caspase-$1^{-/-}$ mice (KO) or wildtype (WT) mice. BMC reconstitution was confirmed at 8 weeks. 1–3 $\times 10^{5}$ B16 (left upper panel) or Panc02 (right upper panel) cells were subcutaneously

injected to the right flank area and the injected tumor was measured daily. Bottom graphs: Tumor volume. $CD3^+$ T cells were depleted via antibody depletion i.p. twice a week in chimeric C57BL/6 mice adoptively transferred with BMCs from caspase-1 KO or WT mice. Wildtype $Gr\text{-}1^+CD11b^+$ MDSCs (enriched from splenocytes of tumor-bearing wildtype mice) were transferred into tumor-bearing chimeric mice (left lower panel). MDSCs were also treated thalidomide (50 μg/mL) prior to MDSC transfer in some groups (right lower panel). $*P<0.05$, $**P<0.01$.

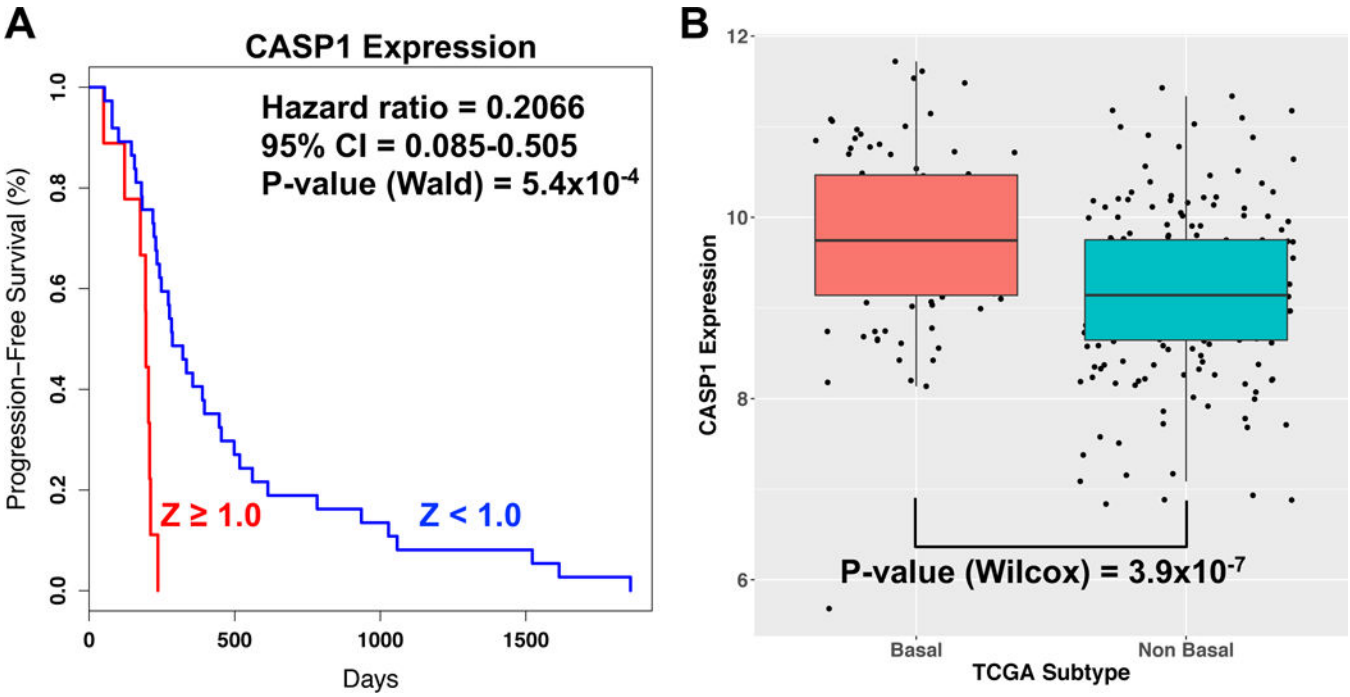

Figure 5. Increased caspase-1 expression is associated with worse prognosis in a TCGA HNSCC dataset.

Analysis of TCGA data for caspase-1 gene expression in HNSCC patients. (A) Kaplan-Meier showing progression-free survival. Of 46 patients for whom CASP1 gene expression and progression-free survival data were available, nine were defined as overexpressing CASP1 (Z-score ≥ 1.0; red line) and 36 were defined as have wild-type expression (Z-score < 1.0; blue line). Red line: Caspase-1 high; Blue line: Caspase-1 low. Elevated caspase-1 expression is significantly associated with the HNSCC basal subtype (B). Box plot of caspase-1 expression in basal and non-basal subtypes. Boxplots show the interquartile range (IQR; box height) with the upper horizontal line showing the 75% quantile, lower showing the 25% quantile, and center line representing the median. The vertical line (whisker) extends below the lower quantile (LQ) to minimum of LQ – (1.5 * IQR) and extends above the upper quantile (UQ) to a maximum of UQ – (1.5 * IQR). Data points show patients outside of the IQR. A Z-score cutoff of ≥ 1.0 was used to define patients as overexpressing caspase-1 (see *Materials and Methods*). CI: confidence interval.

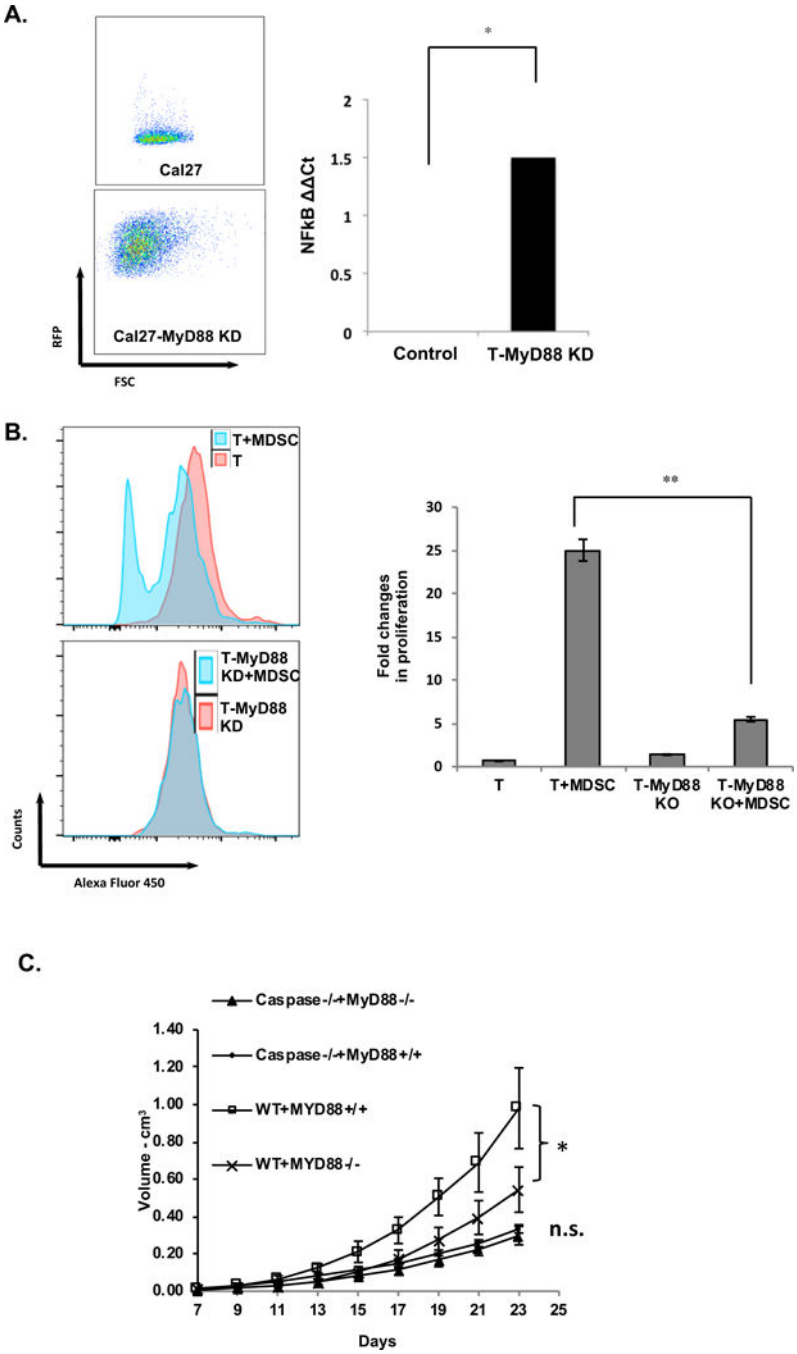

Figure 6. Caspase-1 from myeloid cells induces tumor proliferation via MyD88 oncogenic signaling.

(A) Cal27 cells were transduced with MyD88 siRNA lentivirus (MyD88 knockdown (KD)) and probed for NFkB expression via qPCR. Left panel: transduction efficiency of the reporter RFP gene in Cal27 with and without MyD88 KD. Right panel: Relative NFkB gene expression between the control Cal27 cells (transduced with scrambled lentivirus) and MyD88 knockdown Cal27 cells (T-MyD88 KD). Higher ΔΔCt value represents greater cycling which inversely reflects low expression of gene. (B) Sorted human MDSCs were cocultured with Cal27 cells with and without MyD88 knockdown, and tumor cell

proliferation was assessed. Representative histogram plots of Cal27 proliferation under different conditions shown (left) in addition to fold change in proliferation (right). $^{**}P<0.01$. (C) *In vivo* tumor growth curve of B16 and MyD88 KD-B16 cells in caspase-1 null chimeric mice (all with T-cell depletion). $^{*}P<0.05$; n.s. – not significant. Each of the *in vitro* experiments were repeated at least 3 times independently. Error bars in panels B represent SEM from triplicates.